

Unravelling relativistic fermions in Weyl semimetal TaAs by magnetostriction measurements

T. Cichorek,¹ L. Bochenek,¹ J. Juraszek,¹ Yu. V. Sharlai,² and G. P. Mikitik²

¹*Institute of Low Temperature and Structure Research, Polish Academy of Sciences, 50-422 Wrocław, Poland*

²*B. Verkin Institute for Low Temperature Physics and Engineering,
Ukrainian Academy of Sciences, Kharkov 61103, Ukraine*

(Dated: June 14, 2021)

In the topological semimetals, electrons in the vicinity of the Weyl or Dirac nodes behave like massless relativistic fermions that are of interest both for basic research and future electronic applications. Thus far, a detection of these Dirac or Weyl quasiparticles in topological semimetals is often elusive since in these materials, conventional charge carriers exist as well. Here, considering a prototype topological Weyl semimetal TaAs as an example, we show that when the massless quasiparticles reach the ultra-quantum limit in high magnetic fields, the magnetostriction of the semimetal is appreciably produced by the relativistic fermions. This field-induced expansion measured along the [001] direction exhibits a weak dependence on the magnetic-field orientation and is in striking contrast to the magnetostriction measured along the [100] axis. The latter quantity experiences immense changes from large positive to large negative values with minute deviations of the applied field from the [001] direction. Employing a rigid-band approximation, we work out a theory of the magnetostriction for the Weyl semimetals and point out the features of this thermodynamic probe that can serve as hallmarks of the Weyl quasiparticles. Using the theory, we quantitatively describe a part of the obtained experimental data and find a number of the parameters characterizing this material. The derived dependence of the Fermi level on the magnetic field should be also relevant to understanding some other field-dependent properties of TaAs, in particular, the negative longitudinal magnetoresistance. Our results illustrate how a magnetostriction may be used to unveil Weyl fermions in topological semimetals with a noncentrosymmetric crystal structure.

For a long time, a study of relativistic quasiparticles has been limited to the high-energy physics until groundbreaking experiments regarding the two-dimensional material graphene [1]. This single-layer allotrope of carbon is a zero-gap semiconductor with a linear energy dispersion of conduction and valence bands connected one with the other at their extremities, and thus giving rise to the presence of low-energy quasiparticles governed by the relativistic Dirac equation [2]. Even more promising for quantum information processing are certain three-dimensional semimetals with non-trivial topology that host massless chiral fermions as quasiparticle excitations described by the relativistic Weyl equation [3, 4]. Due to the breaking of either the time-reversal symmetry or the inversion symmetry, a Weyl semimetal is characterized by the band-touching points known as Weyl nodes around which the singly degenerate bands disperse linearly in all three momentum space directions [5].

Because of the intrinsic chirality of Weyl quasiparticles and the emerged monopole-like structure of the Berry curvature, topological semimetals promise the wealth of novel phenomena. In particular, the surface Fermi arcs are recognized as prime direct characteristics of the Weyl semimetal [5]. The negative longitudinal magnetoresistance [6–9] caused by the chiral anomaly, and unusual quantum oscillations produced by a cyclotron motion that weaves together the Fermi arcs and chiral bulk states [10, 11] are other inherent properties of these materials. Berry’s “monopoles” give rise to a phase shift in any quantum oscillations associated with Weyl Fermi pockets, and so measurements of this shift are widely used now to detect Weyl fermions (see, e.g., Refs. [114–119] in review [12]). Recently, a unique type of acoustic collective mode called chiral zero sound has been theoretically proposed for Weyl semimetals with multiple pairs of Weyl nodes [13], and giant

quantum oscillations of the thermal conductivity discovered in the prototypical Weyl semimetal TaAs have been explained with this chiral sound [14]. Besides, the magnetic susceptibility measurements appears to be a useful probe for discerning the relativistic quasiparticles [12, 15, 16]. However, most of these experimental signatures of the Weyl fermions are subtle and indirect especially if they coexist with conventional “trivial” quasiparticles. For example, although the negative longitudinal magnetoresistance in a parallel magnetic field was observed in a number of Weyl semimetals, its interpretation as the long-sought manifestation of the chiral anomaly remains controversial in view of a possible experimental artifact [17, 18]. Therefore, new routes to detect experimental signatures of relativistic quasiparticles in topological semimetals are highly awaited.

In this article, we demonstrate that measuring the field-induced length change $\Delta L/L$ of a topological semimetal, one can distinguish between relativistic and trivial electrons because this thermodynamic probe for linearly crossing bands cardinally differs from the magnetostriction for trivial parabolic bands in the ultra-quantum limit when the magnetic field is so high that the appropriate quantum oscillations disappear. Furthermore, the magnetostriction at experimentally accessible magnetic fields is larger for a small electron pocket than for a large electron group that usually gives a prevailing contribution to other physical quantities and can mask the Weyl electrons. Additional specific feature of the magnetostriction in the low-field range is its extreme sensitivity to the position of electron Fermi level E_F and the concomitant sharp change of its sign when E_F crosses the energy of the Weyl point.

To illustrate differences in the field-induced length change caused by relativistic fermions and conventional charge carri-

ers, we take TaAs as an example. Tantalum arsenide crystallizes in a body-centered tetragonal structure that lacks a horizontal mirror plane and thus the inversion symmetry. This noncentrosymmetric structure is essential to the existence of multiple pairs of the Weyl nodes divided into four pairs of the W1 points and eight pairs of the W2 points [3]. It is remarkable that the Fermi level E_F in TaAs is sufficiently close to the energies of these Weyl points in order to generate chiral quasiparticles at the Fermi surface. In addition to this, the cross-sectional areas of both the W1 (banana shaped) and W2 (nearly isotropic sphere) pockets are so small that the ultra-quantum limit for the Weyl electrons can be easily reached in experiments [18, 19]. These electron pockets coexist with trivial hole pockets aligned along the nodal rings which would occur in TaAs if the spin-orbit interaction were absent [19].

RESULTS

Magnetostriction of Noncentrosymmetric Weyl Semimetals. The magnetostriction of nonmagnetic conductive materials is directly related to the density of the charge carriers in them. In particular, a pocket i of the Fermi surface gives the following contribution to the magnetostriction:

$$\frac{\Delta L}{L} = \Lambda_i (n_i(H) - n_i(0)), \quad (1)$$

where $n_i(H)$ is the H -dependent density of the charge carriers in this pocket, and the constant Λ_i depends on the direction along which the length change ΔL is measured. Formula (1) results from a minimization of the total energy consisting of the elastic energy proportional to $(\Delta L/L)^2$ and of the electron energy that is determined by the density n_i of the charge carriers. This formula is written under the assumption that a deformation of the crystal shifts the appropriate electron band as a whole and does not change its shape. As a rule, this rigid-band approximation is well justified. That is why the magnetostriction is very small [20] if all charge carriers belong to a single band. [In this case formula (1) predicts that the magnetostriction vanishes since $n_i(H) = n_i(0)$ due to the conservation of the carriers]. On the other hand, for a multiband material with multivalley structure such as pure Bi, this thermodynamic quantity is greatly enhanced ($\sim 2 \times 10^{-6}$ at 10 T [21, 22]) due to a band overlap and an electron redistribution between the bands at the switching-on of the magnetic field.

Distinctions between the Weyl and trivial electrons. Let us compare the magnetostrictions produced by the Weyl quasiparticles and by the trivial electrons for which the spectrum has the parabolic form. For trivial electrons in strong magnetic fields H , their lowest Landau level rises above the Fermi level if the parameter δ characterizing the electron magnetic moment $\mu_e = \delta(e\hbar/m_*c)$ is less than $1/2$ where m_* is the cyclotron mass. This moment consists of its spin and orbital parts, the latter being due to the spin-orbit interaction. For such fields, the Fermi-surface pocket i of the trivial electrons

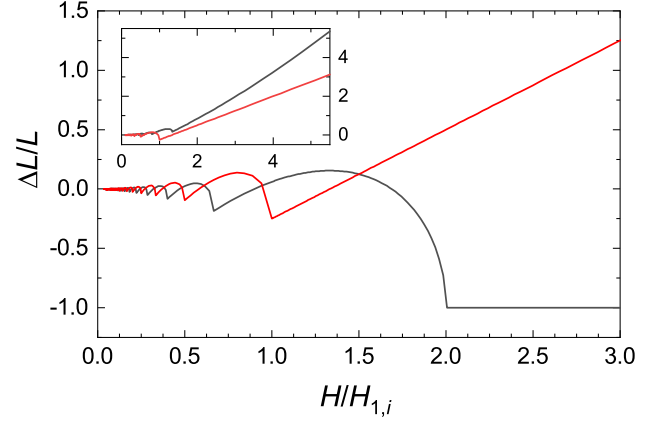


FIG. 1. **The magnetostriction of the Weyl electrons (red) and of the trivial electrons with parabolic spectrum (black) versus magnetic field H at zero temperature.** Here $H_{1,i}$ is defined by Eq. (3), the magnetostriction $\Delta L/L$ (per $\Lambda_i n_i(0)$) is calculated with equations of Supplemental Notes 2 and 3. For the trivial electrons, the parameter δ is assumed to be equal to zero. Note the relative phase shift of the oscillations shown by the red and black curves. Inset: The similar plot, but when $\delta = 0.75$ for the trivial electrons (black dashed line). In this case $\Delta L/L$ (per $\Lambda_i n_i(0)$) = $(0.75u^{-3/2} \sqrt{u + \delta} - 0.5 - 1)$ for $H > H_{1,i}/(1.5 - \delta)$ where $u \equiv H_{1,i}/H$.

empties, and $n_i(H) = 0$ in this ultra-quantum limit. Thus, the magnetostriction of these electrons becomes constant,

$$\frac{\Delta L}{L} = -\Lambda_i n_i(0) \equiv a_i. \quad (2)$$

This saturation of the magnetostriction takes place at $H > H_{1,i}/(0.5 - \delta)$, see Fig. 1, where

$$H_{1,i} = \frac{cS_{\max,i}}{2\pi e\hbar} \quad (3)$$

is frequency of the quantum oscillations occurring at $H < H_{1,i}$, and $S_{\max,i}$ is the maximal cross-sectional area of the pocket i . On the other hand, if $\delta > 1/2$, the H -dependent displacement $(e\hbar/2m_*c)H$ of the lowest Landau level from the band edge ε_0 is less than the electron Zeeman energy $\mu_e H$, and at least one Landau level remains occupied by the charge carriers at any H . In this case,

$$\frac{\Delta L}{L} \approx a_i + \gamma_i H^{3/2}, \quad (4)$$

for the magnetic fields $H \gg H_{1,i}$, with the factor γ_i being dependent on δ (Fig. 1).

In the weak magnetic fields $H \ll H_{1,i}$, if the quantum oscillations are suppressed by impurities or a temperature, the magnetostriction takes the form

$$\frac{\Delta L}{L} = -a_i \frac{3H^2}{8H_{1,i}^2} \left(\delta^2 - \frac{1}{12} \right) \equiv c_i H^2. \quad (5)$$

If the oscillations are superimposed on a smooth background, this formula just describes this background.

In the case of the Weyl electrons, the zero Landau level coincides with the energy of the Weyl point for any H . Therefore, in the ultra-quantum regime when $H > H_{1,i}$, only this level is occupied by the electrons, their density $n_i(H)$ is proportional to H , and the magnetostriction is described by the formula

$$\frac{\Delta L}{L} = a_i \left(1 - \frac{3H}{4H_{1,i}} \right) \equiv a_i + b_i H, \quad (6)$$

where $a_i = -\Lambda_i n_i(0)$, the field $H_{1,i}$ is still defined by formula (3) and coincides with the frequency of the quantum oscillations. A comparison of Eq. (6) with the formulas (2) and (4) for the parabolic spectrum illustrates (cf. Fig. 1) that in the high-field region, the magnetostriction produced by Weyl electrons essentially differs from the magnetostriction of the trivial electrons. For the Weyl electrons, the ratio $a_i/b_i = -4H_{1,i}/3$ of the constant and linear in H contributions to the magnetostriction permits one to evaluate the extremal cross-sectional area of the appropriate pocket even if the quantum oscillations are suppressed by the temperature or by the impurities. In the weak magnetic fields $H \ll H_{1,i}$, the magnetostriction of the Weyl electrons takes the form coinciding with Eq. (5) at the demarcative value of $\delta = 1/2$,

$$\frac{\Delta L}{L} = -\frac{a_i H^2}{16H_{1,i}^2} \equiv c_i H^2. \quad (7)$$

It is clear from formulas (2)–(7) that fits of the quadratic function cH^2 to the smooth background in the weak-field range and of a linear polynomial or a power function to the magnetostriction in the ultra-quantum regime allow one not only to detect the Weyl electrons but also to estimate the parameters $a_i, H_{1,i}$ from experimental data.

We also note that the Weyl and trivial electrons produce strong dependences of their magnetostriction on the Fermi energy E_F . As an example, let us consider these E_F -dependences for the weak magnetic fields and at zero temperature. In the case of the trivial electrons, one has $n_i \propto |E_F - \varepsilon_0|^{3/2}$, $H_{1,i} \propto S_{\max,i} \propto |E_F - \varepsilon_0|$, and hence Eq. (4) yields

$$\begin{aligned} c_i &\propto |E_F - \varepsilon_0|^{-1/2} \propto n_i^{-1/3}, & E_F > \varepsilon_0, \\ c_i &= 0, & E_F < \varepsilon_0, \end{aligned} \quad (8)$$

where ε_0 is the edge of the energy band. (For the trivial holes the same formulas hold true but at the opposite relations between E_F and ε_0). The E_F -dependence of c_i for the Weyl electrons is even more pronounced since $n_i \propto (E_F - \varepsilon_d)^3$, $H_{1,i} \propto S_{\max,i} \propto (E_F - \varepsilon_d)^2$ in this case, and hence Eq. (7) gives

$$c_i \propto \pm |E_F - \varepsilon_d|^{-1} \propto n_i^{-1/3}, \quad (9)$$

where ε_d is the energy of the Weyl point, and the signs \pm correspond to the electrons ($E_F > \varepsilon_d$) and holes ($E_F < \varepsilon_d$), respectively.

We emphasize that the formulas (8) and (9) imply a similar increase of the coefficient c_i with decreasing the charge-carrier

density n_i for both the trivial and Weyl electrons. The difference between these charge carriers is only that the function $c_i(E_F)$ changes its sign at the energy of the Weyl point ε_d , whereas this change does not occur for the trivial electrons. More importantly, however, the relation $c_i \propto n_i^{-1/3}$ reveals that the magnetostriction is substantially larger for a small electron pocket than for a large electron group. This feature is a manifestation of the fact that the magnetostriction is not proportional to $\nu_i = dn_i(E_F)/dE_F$, the density of states of the appropriate charge carriers. This ν_i increases as $n_i^{1/3}$ for the trivial electrons and as $n_i^{2/3}$ in the case of the Weyl quasiparticles.

Advantages of the magnetostriction. The aforementioned features of the magnetostriction makes it a useful tool for studying topological semimetals if the Weyl points are in the vicinity of E_F . Indeed, the experimental signatures for the Weyl fermions in the electrical-resistivity measurements are extensively masked by the contribution of a large pocket of trivial charge carriers even if these carriers have a smaller velocity. Essentially the same holds true for any other physical quantity that is proportional to the density of electron states.

Let us compare now the magnetostriction with the magnetization, the orbital part of which is not determined by the density of electron states as well, and which is considered as another thermodynamic probe of the Weyl electrons [12, 15, 16]. In the ultra-quantum limit, the magnetization of the Weyl electrons is proportional to $H \ln(CH/H_{1,i}) - 6H_{1,i}$ where C is a constant [12, 23], see also [15, 16]. The magnetization of the trivial electrons in this limit tends to zero [16] if the parameter $\delta < 1/2$ and, as can be shown, is proportional to $H^{3/2}$ if $\delta > 1/2$. In other words, the results for the magnetostriction and the magnetization are quite similar. However, a large electron group (or even a filled energy band) gives a large contribution to the magnetization that is proportional to H for the magnetic fields at which the Weyl electrons are in the ultra-quantum regime. This linear term in the magnetization is practically indistinguishable from the term $M \propto H \ln(H/H_{1,i})$ produced by the Weyl electrons since the factor $\ln(H/H_{1,i})$ does not exhibit an essential variation in accessible fields $H > H_{1,i}$. To extract reliably the Weyl-electron contribution to the magnetization, it is necessary to carry out an additional subtraction of extrapolated low-field magnetization from the high-field experimental data [12].

A measurement of the magnetic torque is the effective way of determining the transverse component of the magnetization [15, 16]. However, this component and the magnetic torque vanish when the magnetic fields is aligned with a symmetry axis of a crystal. At magnetic fields tilted away from the symmetry axis, even equivalent pockets in a Weyl semimetal produce different contributions to the magnetization and to the magnetostriction, and an analysis of these quantities becomes complicated for the semimetals with multiple Weyl nodes. However, the magnetostriction (and the longitudinal magnetization) remains nonzero at the magnetic field aligned with the symmetry axis, and such types of the experiments are most

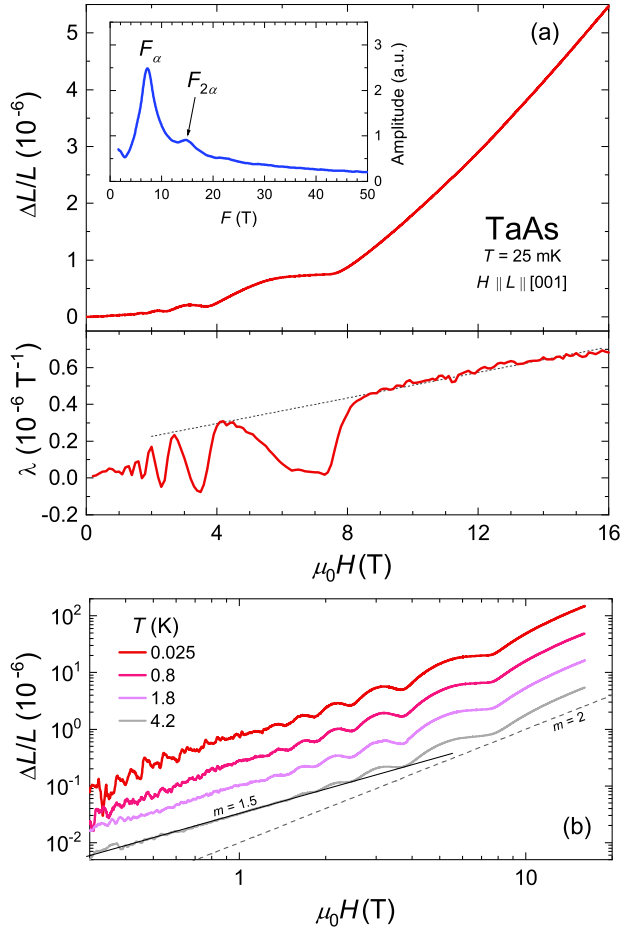


FIG. 2. **Magnetostriction in the Weyl semimetal TaAs.** (a) Top: Magnetic-field dependence of the relative length change $\Delta L/L$ of sample 1 measured along the [001] direction at 25 mK in the parallel configuration ($H \parallel \Delta L$). Inset: The Fourier transform of the oscillatory magnetostriction obtained by subtracting the smooth background $c_b H^2$ with $c_b = 1.79 \cdot 10^{-8} \text{ T}^{-2}$ from the experimental data of the main panel. Bottom: Corresponding magnetostriction coefficient $\lambda \equiv (1/L)dL/dB$. (b) A log-log graph of the c -axis magnetostriction measured at different temperatures up to 4.2 K. Curves are offset for clarity. Note the slopes clearly distinct from the quadratic ($m=2$) behavior expected for the magnetic fields $H \ll H_1$. The black dashed and straight solid lines correspond to the functions H^m .

convenient for detecting the Weyl fermions.

Magnetostriction of TaAs along the [001] direction. Let us exemplify the above considerations by an investigation of the field-induced length change of the Weyl semimetal TaAs, which has relatively simple Fermi-surface topology, combined with small extremal cross sections. When the magnetic field H is parallel to the c axis of TaAs, all the pockets in the W1 and W2 electron groups and in the group of the holes remain equivalent. Let $H_{1,W1}$, $H_{1,W2}$, and $H_{1,h}$ denote the fields H_1 at which the W1 and W2 electrons pockets and the holes enter the ultra-quantum regime, respectively. For this direction of H , according to Ref. [19], one has $H_{1,W1} \sim 7$

T, $H_{1,W2} \sim 5$ T, and the field $H_{1,h} \sim 19$ T for the holes is larger than the maximal field of 16 T in our experiments. The latter implies that the range $H \leq 16$ T can be considered as the low-field region for the holes.

Figure 2(a) shows the magnetostriction of TaAs (sample 1) measured along the [001] direction at 25 mK. The field-induced expansion is large and the relative length change $\Delta L/L$ amounts to about 5.5×10^{-6} at $H = 16$ T. With the magnetic field aligned along the c axis, the quantum oscillations reaching large amplitudes ($\sim 30\%$ of the background signal at 3 T) are observable in the raw $\Delta L/L$ data (top panel) and even more sharply discernible in the derived coefficient $\lambda = \frac{1}{L} \frac{dL}{dB}$ (bottom panel) that represents the derivative of the charge-carrier density with respect to the magnetic field. The sharp change observed in λ at 7.5 T and the linearly increasing signal at higher fields clearly show that the W1 and W2 electron groups enter the ultra-quantum regime, and the magnetostriction above 8 T is well approximated by the square polynomial $a + bH + c_h H^2$ (the fit gives $a \approx -2.18 \times 10^{-6}$, $b \approx 2.55 \times 10^{-7} \text{ T}^{-1}$, $c_h \approx 1.49 \times 10^{-8} \text{ T}^{-2}$). The presence of a linear in H term in the magnetostriction clearly indicates the existence of the Weyl electrons, whereas the term $c_h H^2$ may be associated with the holes that are in the low-field range, $H < H_{1,h}$. Thus, the presented experimental data do demonstrate the possibility of detecting the relativistic fermions with the magnetostriction.

Finally we note that except for the oscillatory features, the overall H -dependence of the c -axis magnetostriction remains essentially unaltered up to the temperature 4.2 K [cf. Fig. 2(b)]. However, the log-log graph seems to reveal a deviation of this H -dependence from the H^2 law expected in the low-field region (black solid line). This finding might point to a very small value of the field $H_{1,W2}$. On the other hand, however, the deviation of the H -dependence from a quadratic behavior is less than or of the order of 10^{-8} , and hence a detailed insight into the low-field region would require much larger TaAs crystals.

Analysis of the magnetostriction for TaAs. The density $n_i(H)$ of the Weyl quasiparticles can be calculated at an arbitrary value of H . This permits us to describe quantitatively the experimental data for the magnetostriction of TaAs. We find that at $H_{1,W1} = 7.2$ T, the frequency of the calculated oscillations in the magnetostriction coincides with that observed experimentally. Since this frequency agrees with $H_{1,W1} = 7 \pm 0.5$ T reported by Arnold et al. [19], we conclude that the Fermi-surface parameters in both the samples are close to each other, and we may be guided by the data of Ref. [19] in our analysis. The oscillations with the frequency $H_{1,W2}$ do not manifest themselves in our data, and we take the value $H_{1,W2} = 5$ T to maintain agreement with the results of Arnold et al. [19]. Then, using formula (6) and the values of the constants a and b found above from the approximation of the magnetostriction in the high-field range, we arrive at the two linear equations in the parameters a_{W1} and a_{W2} characterizing the W1 and W2

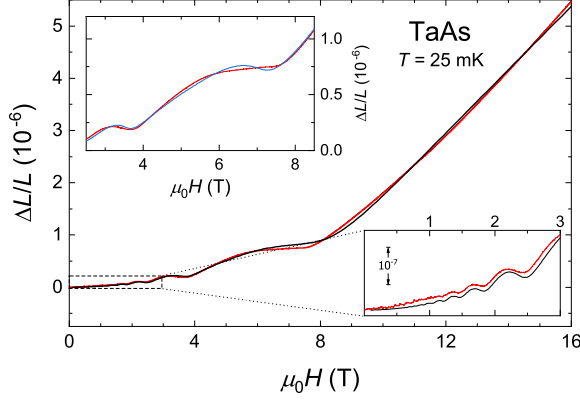


FIG. 3. **Comparison of the calculated magnetostriction with the experimental data for TaAs.** The red line shows the c -axis magnetostriction $\Delta L/L$ of the crystal TaAs measured at $T = 25$ mK, see Fig. 2(a). The black line depicts the magnetostriction calculated at zero temperature and at the values of the parameters presented in Table I (set No. 1). The lower inset shows the magnetostriction in the enlarged scale for $0 < \mu_0 H < 3$ T. In the upper inset, the experimental data (the red line) are compared with the magnetostriction calculated at a constant chemical potential, $\zeta = \zeta_0$, (the blue line); see also the text.

electrons,

$$\begin{aligned} a_{W1} + a_{W2} &= a, \\ -0.75 \left(\frac{a_{W1}}{H_{1,W1}} + \frac{a_{W2}}{H_{1,W2}} \right) &= b. \end{aligned}$$

These equations give $a_{W1} \approx -1.58 \cdot 10^{-6}$, $a_{W2} \approx -0.60 \cdot 10^{-6}$. With these parameters, we calculate the magnetostriction of the Weyl electrons at zero temperature T in the whole interval of the magnetic fields, $0 \leq H \leq 16$ T. To fit the magnitude of calculated oscillations to the experimental data, we use the dimensionless parameter specifying the scattering of the W1 electrons by impurities, $\gamma_{W1} = \pi T_{D,W1}/(E_F - \varepsilon_{d,W1})$, and find from the fit that $\gamma_{W1} = 0.025$ where $\varepsilon_{d,W1}$ is the energy of the Weyl points W1, and $T_{D,W1}$ is the Dingle temperatures for the W1 electrons. The similar ratio $\pi T_{D,W2}/(E_F - \varepsilon_{d,W2})$ for the W2 electrons is assumed to be equal to 0.1 in order to suppress the oscillations associated with these quasiparticles. (The exact value of this ratio cannot be found since the appropriate oscillations are unobservable in our experiments.) Adding the hole contribution $c_h H^2$ to the calculated magnetostriction of the Weyl electrons, we find that the theoretical curve sufficiently well reproduces the experimental data in the whole interval $0 < H < 16$ T. In Fig. 3 (the upper inset), we show the calculated and experimental curves in the range 2.5 T $< H < 8.5$ T where the discrepancy between them is maximal.

The above theoretical analysis of the magnetostriction is based on formulas obtained under the assumption of independence of the Fermi energy E_F on the magnetic field H . This situation does can occur in a conductive material when it con-

tains a large charge-carrier group that maintains the constancy of E_F . However, in TaAs all the electron and hole pockets are relatively small. In this case, a consideration must be given to the magnetic-field dependence of E_F (i.e., of the chemical potential ζ if the temperature is nonzero) in analyzing the magnetostriction. This dependence $\zeta(H)$ can be found from the conservation condition of the total charge-carrier density,

$$\sum_i (n_i(\zeta, H) - n_i(\zeta_0, 0)) = 0, \quad (10)$$

where i runs all the electron and hole pockets, and ζ_0 is the value of the chemical potential at $H = 0$. Since the dispersion law for the holes need not be well described by a simple parabolic dependence, we use the expression for $n_h(\zeta, H) - n_h(\zeta_0, 0)$ that is valid in the low magnetic fields ($H < H_{1,h}$) at any dispersion of these charge carriers,

$$\begin{aligned} n_h(\zeta, H) - n_h(\zeta_0, 0) &= n_h(\zeta, H) - n_h(\zeta, 0) + n_h(\zeta, 0) - n_h(\zeta_0, 0) \\ &\approx H^2 \left(\beta(\zeta_0) + \frac{d\beta(\zeta_0)}{d\zeta_0} (\zeta - \zeta_0) \right) + \nu_h(\zeta_0) (\zeta - \zeta_0), \end{aligned}$$

where $\nu_h = \partial n_h(\zeta, 0)/\partial \zeta$ is the density of states for the holes in zero magnetic field, whereas the function $\beta(\zeta)$ defines the variation of the hole density in the low magnetic fields, $n_h(\zeta, H) - n_h(\zeta, 0) = \beta(\zeta) H^2$ [i.e., $\beta = c_h/\Lambda_h$ where c_h has been introduced above].

Using equation (10), one can express the contribution of the holes, $\Lambda_h (n_h(\zeta, H) - n_h(\zeta_0, 0))$, to the total magnetostriction $\Delta L/L$, Eq. (1), in terms of the contributions of the W1 and W2 electrons, and we arrive at

$$\frac{\Delta L}{L} = \sum_i (\Lambda_i - \Lambda_h) (n_i(\zeta, H) - n_i(\zeta_0, 0)), \quad (11)$$

where i runs only the electron pockets. With formulas (10) and (11) written in the case when H is parallel to the c axis, we calculate the magnetostriction in the whole magnetic-field interval, $0 < H < 16$ T. As in the simplified approach when $\zeta(H) = \zeta_0$, these formulas are determined by $H_{1,W1}$, $H_{1,W2}$, and by the dimensionless parameters specifying the scattering of the W1 and W2 electrons by impurities, $\gamma_{W1} = \pi T_{D,W1}/(\zeta_0 - \varepsilon_{d,W1})$ and $\gamma_{W2} = \pi T_{D,W2}/(\zeta_0 - \varepsilon_{d,W1})$. Besides this, the magnetostriction is also proportional to the constants $A_{W1} = -(\Lambda_{W1} - \Lambda_h) n_{W1}(\zeta_0, 0)$ and $A_{W2} = -(\Lambda_{W2} - \Lambda_h) n_{W2}(\zeta_0, 0)$ that replace $a_{W1} = -\Lambda_{W1} n_{W1}(\zeta_0, 0)$ and $a_{W2} = -\Lambda_{W2} n_{W2}(\zeta_0, 0)$ introduced above. As to the chemical potential $\zeta(H)$, it depends on the ratio $n_{W2}(\zeta_0, 0)/n_{W1}(\zeta_0, 0)$ and on the above-mentioned β , $d\beta/d\zeta$, ν normalized to $n_{W1}(\zeta_0, 0)$, i.e., on the following quantities:

$$\begin{aligned} \tilde{\beta}_0 &\equiv -\frac{\beta(\zeta_0)}{n_{W1}}, \\ \tilde{\beta}_1 &\equiv -\frac{(\zeta_0 - \varepsilon_{d,W1})}{n_{W1}} \frac{d\beta(\zeta_0)}{d\zeta_0}, \\ \tilde{\nu}_h &\equiv -\frac{(\zeta_0 - \varepsilon_{d,W1})}{n_{W1}} \nu_h(\zeta_0). \end{aligned}$$

In Fig. 3 we compare the magnetostriction calculated at $T = 0$ with the experimental data shown in Fig. 2. The agreement between them improves as compared to the case of the

TABLE I. The values of the parameters for the calculation of the magnetostriction $\Delta L/L$ along the c axis at H aligned with this axis and at $(\zeta_0 - \varepsilon_{d,W1})/(\zeta_0 - \varepsilon_{d,W2}) = 2.5$, $n_{W2}/n_{W1} = 0.15$.

#	$H_{1,W1}$ T	$H_{1,W2}$ T	$\tilde{\nu}_h$	$\tilde{\beta}_0$ 10^{-3}T^{-2}	$\tilde{\beta}_1$ 10^{-3}T^{-2}	A_{W1} 10^{-6}	A_{W2} 10^{-6}	γ_{W1}	γ_{W2}
1	7.2	5	-0.91	1.63	1.53	-10.9	-1.92	0.025	0.04
2	7.2	1.35	-1.39	5.93	1.34	-4.72	-0.43	0.025	0.04

constant chemical potential because of the change in the shape of the last two oscillations at $3 \text{ T} < H < 8 \text{ T}$. The derived dependence of the chemical potential on the magnetic field H is presented in Fig. 4. It is seen that due to condition (10), the largest electron group W1 induces the oscillation with the same frequency 7.2 T for the other charge carriers. The values of the parameters (Table I) have been chosen so that the calculated magnetostriction best matches the experimental data at the fixed values of $(\zeta_0 - \varepsilon_{d,W1})/(\zeta_0 - \varepsilon_{d,W2})$ and n_{W2}/n_{W1} where $\varepsilon_{d,W2}$ is the energy of the Weyl points W2. Let us now comment on the first set of the parameters presented in Table I. The second set will be discussed in the next section.

Applying formulas of Ref. [24] to the data of Ref. [19] on the cross-sectional areas and cyclotron masses of the electrons and holes, we find the density $n_{W1} \approx 2.5 \cdot 10^{18} \text{ cm}^{-3}$, the ratio $n_{W2}(\zeta_0, 0)/n_{W1}(\zeta_0, 0) \sim 0.15$, and the position of the chemical potential ζ_0 relative to the energies ε_{W1} , ε_{W2} : $\zeta_0 - \varepsilon_{d,W1} \approx 28.4 \pm 3.5 \text{ meV}$ and $\zeta_0 - \varepsilon_{d,W2} \approx 11.9 \pm 1 \text{ meV}$. These values of the parameters have permitted us to set $n_{W2}(\zeta_0, 0)/n_{W1}(\zeta_0, 0) = 0.15$ and $(\zeta_0 - \varepsilon_{d,W1})/(\zeta_0 - \varepsilon_{d,W2}) = 2.5$ in our calculations of the magnetostriction. As in the case of the simplified approach when $\zeta(H) = \zeta_0$, we set $H_{1,W1} = 7.2 \text{ T}$, $H_{1,W2} = 5 \text{ T}$, and the same values of the Dingle temperatures, i.e., $\gamma_{W1} = 0.025$, and $\gamma_{W2} = 0.04$.

If the holes in TaAs can be described by the parabolic spectrum, the parameters $\tilde{\beta}_1/\tilde{\beta}_0$, and $\tilde{\nu}_h$ should be the following:

$$\frac{\tilde{\beta}_1}{\tilde{\beta}_0} = \frac{(\zeta_0 - \varepsilon_{d,W1})}{2(\varepsilon_0 - \zeta_0)},$$

$$\tilde{\nu}_h = -\frac{3|n_h|(\zeta_0 - \varepsilon_{d,W1})}{2n_{W1}(\varepsilon_0 - \zeta_0)} = -\frac{3|n_h|\tilde{\beta}_1}{n_{W1}\tilde{\beta}_0},$$

where ε_0 is the edge of the hole band. Using the values of $\tilde{\beta}_0$ and $\tilde{\beta}_1$ from Table I (set No. 1), we find from the first equality that $\varepsilon_0 - \zeta_0 \approx 15.1 \pm 1.9 \text{ meV}$. This value agrees with the estimate $\varepsilon_0 - \zeta_0 \approx 12.6 \div 16.2 \text{ meV}$ that can be derived from the data of Arnold et al. [19]. From Table I and the second equality, we obtain $|n_h|/n_{W1} \approx 0.32$. This means that the doping in our sample, $n_{W1} + n_{W2} - |n_h|$, is of the order of $0.83n_{W1} \approx 2 \cdot 10^{18} \text{ cm}^{-3}$. As to the value of $\tilde{\beta}_0$ presented in Table I, it can be reproduced with formula (5) at $|n_h|/n_{W1} = 0.32$ and $H_{1,h} = 19 \text{ T}$ if we assume that due to the strong spin-orbit interaction, the magnetic moment of the holes is sufficiently large (the parameter δ amounts to 2.2).

Let us now compare the parameters obtained with and without consideration for the H -dependence of ζ . The definitions

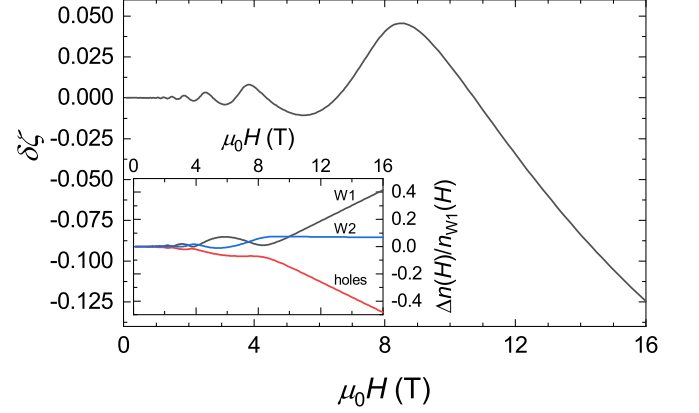


FIG. 4. The shift of the chemical potential relative to its value at zero magnetic field versus H in the TaAs crystal. Here $\delta\zeta \equiv (\zeta(H) - \zeta_0)/(\zeta_0 - \varepsilon_{W1})$, $\zeta_0 \equiv \zeta(0)$. The shift is calculated with equation (10). All the parameters are the same as in Fig. 3. Inset: Dependences of $(n_{W1}(H) - n_{W1}(0))/n_{W1}(0)$, $(n_{W2}(H) - n_{W2}(0))/n_{W1}(0)$, and $(n_h(H) - n_h(0))/n_{W1}(0)$ on $\mu_0 H$. Note that although ζ decreases with H at $\mu_0 H > 8 \text{ T}$, $n_{W1}(H)$ increases in this field region since the growing magnetic field increases the capacity of the Landau levels.

of a_{Wi} and A_{Wi} give

$$\frac{A_{W1}}{a_{W1}} = \frac{\Lambda_{W1} - \Lambda_h}{\Lambda_{W1}}, \quad \frac{A_{W2}}{a_{21}} = \frac{\Lambda_{W2} - \Lambda_h}{\Lambda_{W2}}.$$

These relations together with the values of a_{Wi} and A_{Wi} found above lead to the estimates: $\Lambda_{W1} \approx -0.17\Lambda_h$ and $\Lambda_{W2} \approx -0.45\Lambda_h$. Then, the ratio

$$\frac{A_{W2}}{A_{W1}} = \frac{\Lambda_{W2} - \Lambda_h}{\Lambda_{W1} - \Lambda_h} \left(\frac{n_{W2}}{n_{W1}} \right) \approx 1.24 \left(\frac{n_{W2}}{n_{W1}} \right),$$

which is equal to 0.176 according to Table I, permits us to find the ratio of the densities: $n_{W2}/n_{W1} \approx 0.142$. This value agrees with the estimate presented above and is close to that (0.15) used in our calculations. This fact demonstrates the self-consistency of the chosen parameters and shows that the simplified approach, within which the H -dependence of ζ is neglected, can provide a sufficiently accurate description of the magnetostriction. These conclusions are also supported by the comparison of $c_h \approx 1.49 \cdot 10^{-8}$ found within the simplified approach with the same quantity expressed in terms of A_{W1} and $\tilde{\beta}_0$: $c_h \equiv -\Lambda_h n_{W1} \tilde{\beta}_0 = \Lambda_h A_{W1} \tilde{\beta}_0 / (\Lambda_{W1} - \Lambda_h) \approx 1.52 \cdot 10^{-8}$. Both the approaches also lead to almost the same coefficient c_b in the background term $c_b H^2$ (cf. Fig. 2) on which the oscillations of the magnetostriction are superimposed at $H < 7 \text{ T}$,

$$c_b = c_h - \frac{a_{W1}}{16H_{1,W1}^2} - \frac{a_{W2}}{16H_{1,W2}^2} \approx 1.83 \cdot 10^{-8},$$

$$c_b = -\frac{A_{W1}}{16H_{1,W1}^2} - \frac{A_{W2}}{16H_{1,W2}^2} \approx 1.79 \cdot 10^{-8}.$$

Finally, taking into account that $n_{W1} \approx 2.5 \cdot 10^{18} \text{ cm}^{-3}$, we find from the value of A_{W1} and the above estimates that $\Lambda_h \approx$

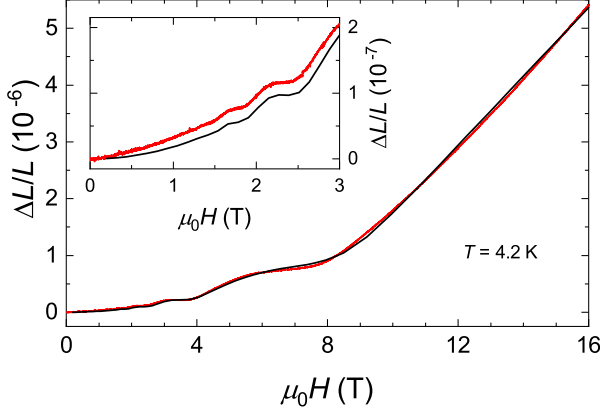


FIG. 5. Comparison of the calculated magnetostriction with the experimental data at $T = 4.2$ K for TaAs. The red line shows the magnetostriction $\Delta L/L$ measured along the c axis at $T = 4.2$ K, see Fig. 2(b). The black line corresponds to the magnetostriction calculated at the dimensionless temperature $t = T/(\zeta_0 - \varepsilon_{W1}) = 0.015$ and at the values of the parameters presented in Table I (set No. 1). Inset: The magnetostriction in the enlarged scale for $0 < \mu_0 H < 3$ T.

$-3.7 \cdot 10^{-24} \text{ cm}^3$, $\Lambda_{W1} \approx 0.63 \cdot 10^{-24} \text{ cm}^3$, and $\Lambda_{W2} \approx 1.7 \cdot 10^{-24} \text{ cm}^3$.

In Fig. 5 we compare the magnetostriction measured at the temperature $T = 4.2$ K [see Fig. 2(b)] with the magnetostriction calculated at a finite dimensionless temperature $t = T/(\zeta_0 - \varepsilon_{W1})$. All the values of the parameters are assumed to be the same as in Fig. 3. The theoretical curve agrees with the experimental data at $t \approx 0.015$. This value of t leads to the independent estimate of $\zeta_0 - \varepsilon_{W1}$: $\zeta_0 - \varepsilon_{W1} \approx 280 \text{ K} \approx 24 \text{ meV}$, which is only a little less than the value $28.4 \pm 3.5 \text{ meV}$ obtained from the data of Arnold et al. [19] in Ref. [24]. We may now estimate the Dingle temperatures $T_{D,Wi} = (\zeta_0 - \varepsilon_{W1})\gamma_{Wi}/\pi$ for the W1 and W2 electrons. The data of Table I and $\zeta_0 - \varepsilon_{W1} \approx 280 \text{ K}$ give $T_{D,W1} \approx 2.2 \text{ K}$ and $T_{D,W2} \approx 3.6 \text{ K}$. This value of $T_{D,W1}$ is comparable with $T_{D,W1} \approx 3.2 \text{ K}$ obtained in Ref. [19].

In numerous experiments (see review [12] and references therein), the phase of quantum oscillations in topological semimetals was measured to distinguish between the Weyl (Dirac) electrons and trivial quasiparticles. Such investigations are based on the fact that in the case of the Weyl electrons, the nonzero Berry phase of the electron orbits in a magnetic field leads to a shift of the phase of the oscillations by π as compared to the phase corresponding to the trivial electrons [12, 25]. Of course, this phase shift should also occur for the oscillations in the magnetostriction. The insets in Figs. 3 and 5 clearly demonstrates that the phase of the oscillations calculated with formulas for the Weyl electrons does coincide with the experimental one. This result confirms the expected shift of the observed oscillations in $\Delta L/L$, and it is an additional manifestation of the Weyl electrons in TaAs. (If the shift were absent, the theoretical and experimental curves would be mutually displaced in phase like the red and black lines in Fig. 1).

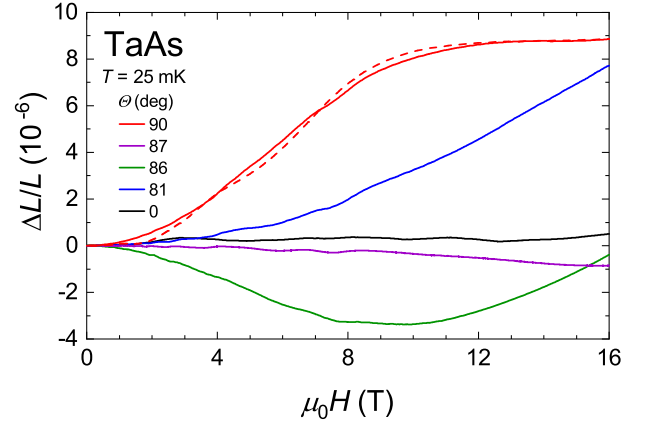


FIG. 6. Angle-dependent magnetostriction of TaAs measured along the a axis. Magnetic-field dependence of the relative length change $\Delta L/L$ of sample 2 is measured along the [100] direction at 25 mK for various angles Θ between the direction of H and the a axis. The magnetic field lies in the plane (010). Note the exceptional changes of $\Delta L/L$ over the small-angle range near $\Theta = 90^\circ$. The red dashed line shows the a -axis magnetostriction that is calculated at $T = 0$ for H aligned with the c axis, using the second set of the parameters in Table I.

DISCUSSION

It is important to note that the values of the parameters $H_{1,W2}$, \tilde{v}_h , $\tilde{\beta}_0$, $\tilde{\beta}_1$, A_{W1} , A_{W2} are not uniquely determined by the fitting of the calculated magnetostriction to the experimental data presented in Figs. 3 and 5. In reality, there is a family of sets of such values. Specifically, it is possible to decrease $H_{1,W2}$ successively and to find sufficiently good fits. (See, e.g., set #2 in Table I.) In choosing the set #1, we are guided by the consistency of the obtained parameters with the results of Ref. [19]. To check the correctness of our choice, we have measured the magnetostriction $\Delta L/L$ along the a axis for the magnetic field still aligned with the c axis. In this case, only the values of A_{W1} and A_{W2} should change due to a change of the constants Λ_{W1} , Λ_{W2} , and Λ_h .

Figure 6 shows the magnetostriction measured along the a axis at $T = 25 \text{ mK}$ (sample 2). We note that a field-induced length change is small ($\sim 0.5 \cdot 10^{-6}$ at $\mu_0 H = 16 \text{ T}$) in magnetic fields applied along the dilatation direction (black curve). In addition, there is a complex $\Delta L(H)/L$ dependence in the entire field range. However, when the dilatometer is rotated by the angle $\Theta = 90^\circ$ to the desired sample orientation $H \parallel c$, the a -axis magnetostriction exhibits a substantial enhancement with a behavior close to the H^2 law between 0.5 and 5 T. This behavior is followed by a tendency to the saturation above about 12 T (red curve). Even more remarkable feature of the a -axis magnetostriction is its high sensitivity to small deviations of the applied field from the [001] direction. Such deviations cause immense changes in the magnetostriction from large positive to large negative values. For example, the violet curve at $\Theta = 87^\circ$ illustrates the field-induced

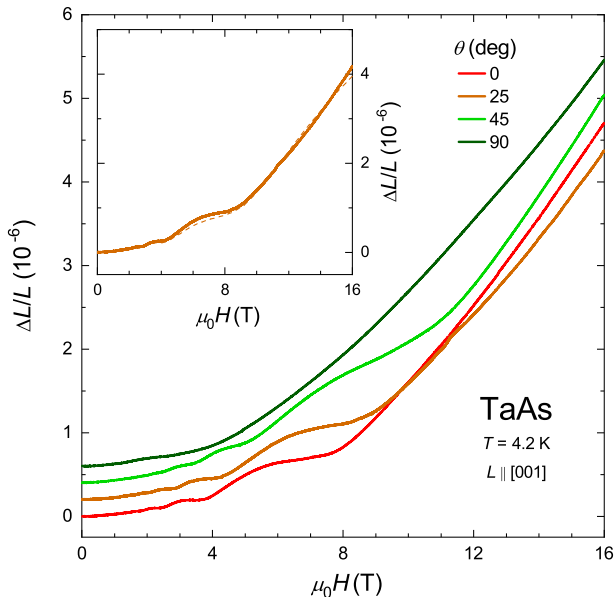


FIG. 7. **Angle-dependent magnetostriction of TaAs measured along the c axis.** Field-induced relative length change of sample 3 along the [001] direction is measured at $T = 4.2$ K and at various angles θ between the direction of the magnetic field and the c axis. The magnetic field lies in the plane (010). For clarity, the different $\Delta L/L$ curves at $\theta > 0$ were shifted subsequently by 0.2×10^{-6} . Inset: The magnetostriction at $\theta = 25^\circ$. The solid line is the experimental data of the main panel, the dashed line shows the calculated magnetostriction.

contraction of TaAs. [Note that Θ is the tilt angle of the applied magnetic field to the a axis in the plane (010), i.e., the case of H directed along the c axis corresponds to $\Theta = 90^\circ$.] This negative magnetostriction is small (close to -1.0×10^{-6} at $\mu_0 H = 16$ T) but shows quantum oscillation at $\mu_0 H \gtrsim 1.2$ T. Moreover, a drastic change of the negative magnetostriction occurs when the magnetic field is just marginally tilted further from the [001] direction ($\Theta = 86^\circ$, green curve). At $\Theta = 81^\circ$ (blue curve), we again observe a large expansion of sample 2.

For comparison, in Fig. 7, we present the angle-dependent magnetostriction of TaAs measured along the c axis at 25 mK (sample 3). Now the tilt angle θ of the magnetic field is measured from the c axis. It is seen that the H -induced length changes do not exhibit any qualitative differences with increasing angle θ .

We have calculated the magnetostriction along the a axis at the magnetic field parallel to the direction [001], using the sets of the parameters presented in Table I, and varying the constants A_{W1} and A_{W2} . For the first set, we are not able to match the theoretical curve with the experimental data. For the second set, the obtained theoretical curve approximately reproduces these data (Fig. 6) if we take $A_{W1} = 15.7 \cdot 10^{-6}$ and $A_{W2} = -2.61 \cdot 10^{-6}$ (beside this, we take the modified values: $\gamma_{W1} = 0.1$, $\gamma_{W2} = 0.08$ since Fig. 2 and 6 show the magnetostrictions for the different samples). However, it is necessary

to emphasize that the second set of the parameters disagrees with the data of Ref. [19]. Apart from the low value of $H_{1,W2}$, the second set leads to $\varepsilon_0 - \zeta_0 \approx 63$ meV, and $|n_h|/n_{W1} \approx 2.05$ (the hole-doped sample). This value of $\varepsilon_0 - \zeta_0$ considerably exceeds the estimate presented above. On the other hand, since the orientation of the magnetic field in our experiments is not established with a high accuracy, and taking into account the high sensitivity of the magnetostriction to this orientation, we cannot be sure that the experimental curve with $\Theta = 90^\circ$ in Fig. 6 really corresponds to the case of H aligned with the c axis. This consideration also argues against set #2 in Table I.

When the magnetic field is tilted away from the c axis in the plane (010), the holes pockets as well as the electron pockets in the W1 and W2 groups become non-equivalent, and one should take into account that with increasing the tilt, the parameters $H_{1,W1}$, $H_{1,W2}$, $\tilde{\beta}_0$, $\tilde{\beta}_1$ not only change in magnitude but their number increases (non-equivalent charge-carrier pockets have different values of these parameters). This makes the strict theoretical analysis of the magnetostriction in the tilted magnetic fields very complicated. As the first attempt in this direction, we have approximately calculated the c -axis magnetostriction at $\theta = 25^\circ$. The result is shown in the inset of Fig. 7.

The quantitative results presented in Fig. 4 clearly demonstrates the essential redistribution of the charge carriers between the bands of the holes and the W1 electrons. In this context, it is worth noting that such a redistribution generally leads to a nonzero longitudinal magnetoresistance of a semimetal if the quasiparticles in its different bands have dissimilar mobilities. Even in the case of the trivial charge carriers when the chiral anomaly is absent, this magnetoresistance can be negative. Indeed, if with increasing H , the trivial electrons of a lower mobility are transferred to another band with higher mobility, the longitudinal conductivity of this material increases (see, e.g. Fig. S10 in Supplemental Material to Ref. [26]). In the case of TaAs, our study reveals that for H parallel to the c axis, both the absolute value $|n_h(H)|$ of the negative hole density n_h and the density of the W1 electrons n_{W1} increase in high magnetic fields (Fig. 4, inset). In this situation, one may expect that the longitudinal conductivity along this axis should increase above about $H = 8$ T for any relation between mobilities of the electrons and holes. Interestingly, the negative magnetoresistance was really observed in TaAs for $E \parallel H \parallel c$ at $7.5 \text{ T} < H < 25 \text{ T}$ in careful measurements using focused-ion-beam lithography to eliminate experimental artifacts due to the current-jetting effect [18].

As for future work, it would be interesting to study in more detail the a -axis magnetostriction in magnetic fields near the c axis and to find more precisely the H -dependence of this quantity at $H \parallel c$. In absence of the experimental information on $H_{1,W2}$, such measurements could enable one to determine unambiguously this parameter characterizing the W2 electrons in TaAs. An interesting issue to explore is also the c -axis magnetostriction in the low magnetic fields for samples larger than ours. In this case, this magnetostriction should be well described by the dependence $c_b H^2$, and the knowledge of

the factor c_b will give a possibility to determine the parameter $H_{1,w2}$ even without a direct measurement of this quantity.

METHODS

Crystal synthesis. TaAs single crystals were synthesized with the chemical vapor transport method following the procedure described elsewhere [27–29]. The chemical composition of the crystals was examined by electron-probe microanalysis with energy-dispersive x-ray spectroscopy. The ratio of 1:0.99 between Ta and As was found, indicating the correct stoichiometric chemical composition. The body centered tetragonal structure (space group $I4_1md$, No. 109) of TaAs single crystals was confirmed by room-temperature x-ray diffraction. No other phases were detected, and the lattice parameters $a = 3.4348 \text{ \AA}$ and $c = 11.6412 \text{ \AA}$ are in good agreement with the literature values [27–29]. The crystal orientation was determined by Laue diffraction.

Sample characterization. All samples (No. 1, No. 2, No. 3) used in this study were obtained from the same growth batch. The residual-resistivity ratio of typical sample $RRR = \rho_{300\text{K}}/\rho_{2\text{K}} \approx 12$ was determined from a zero-field resistance measurement along the c axis. The transverse magnetoresistance MR of about 39 600% was measured at 9 T and 2 K. These parameters are in good agreement with the published literature values, and observed Shubnikov-de Haas oscillations, which were reproduced on multiple samples, point at good quality of our TaAs single crystals.

Magnetostriction measurements. The angle-dependent field-induced length change was measured with a commercial capacitance dilatometer which enables a length resolution of 0.02 \AA [21]. The magnetostriction of the three rectangular TaAs samples having a length of approximately 1.7 mm was studied along the [100] and [001] directions. We performed the magnetostriction measurements down to 25 mK in a dilution refrigerator (Kelvinox 400 HA, Oxford Instruments) inserted into a superconducting magnet for fields up to 16 T. A field-sweep rate as small as 0.5 mTs^{-1} was used, and the highest temperature of our experiments was 4.2 K.

The capacitive dilatometer cell is compact enough to be mounted on an attocube rotator, and thus enables the study of the field-induced length changes as a function of the tilted angle. However, since TaAs single crystals with a typical cross-section of about $0.7 \times 0.9 \text{ mm}^2$ were mounted between two capacitor plates with the diameter of 20 mm, the crystal axis cannot be precisely aligned with the axis of rotation. This type of misalignment can cause the maximum error of 5° .

Numerical calculations. The H -dependences of the magnetostriction for TaAs have been numerically calculated, using our own code elaborated with results of Refs. [30–32].

Acknowledgements. This work was supported by the Polish National Science Centre (Project No. 2016/21/B/ST3/02361).

- [1] Novoselov, K. S. et al. Electric field effect in atomically thin carbon films. *Science* **306**, 666-669 (2004).
- [2] Castro Neto, A. H., Guinea, F., Peres, N. M. R., Novoselov, K. S. & Geim, A. K. The electronic properties of graphene. *Rev. Mod. Phys.* **81**, 109-162 (2009).
- [3] Xu, S.-Y. et al. Discovery of a Weyl fermion semimetal and topological Fermi arcs. *Science* **349**, 613-617 (2015).
- [4] Yan, B. & Felser, C. Topological materials: Weyl semimetals. *Annu. Rev. Condens. Matter Phys.* **8**, 337-354 (2017).
- [5] Armitage, N. P., Mele, E. J. & Vishwanath, A. Weyl and Dirac semimetals in three-dimensional solids. *Rev. Mod. Phys.* **90**, 015001 (2018).
- [6] Parameswaran, S. A., Grover, T., Abanin, D. A., Pesin, D. A. & Vishwanath, A. Probing the chiral anomaly with nonlocal transport in three-dimensional topological semimetals. *Phys. Rev. X* **4**, 031035 (2014).
- [7] Zhang, C. et al. Room-temperature chiral charge pumping in Dirac semimetals. *Nat. Commun.* **8**, 13741 (2017).
- [8] Nielsen, H. B. & Ninomiya, M. The Adler-Bell-Jackiw anomaly and Weyl fermions in a crystal. *Phys. Lett. B* **130**, 389-396 (1983).
- [9] Son, D. T. & Spivak, B. Z. Chiral anomaly and classical negative magnetoresistance of Weyl metals. *Phys. Rev. B* **188**, 104412 (2013).
- [10] Potter, A. C., Kimchi, I. & Vishwanath, A. Quantum oscillations from surface Fermi arcs in Weyl and Dirac semimetals. *Nat. Commun.* **5**, 5161 (2014).
- [11] Moll, P. J. W. et al. Transport evidence for Fermi-arc-mediated chirality transfer in the Dirac semimetal Cd_3As_2 . *Nature* **535**, 266-270 (2016).
- [12] Mikitik, G. P. & Sharlai, Yu. V. Magnetic Susceptibility of Topological Semimetals. *J. Low Temp. Phys.* **197**, 272 (2019).
- [13] Song, Z. & Dai, X. Hear the sound of Weyl fermions. *Phys. Rev. X* **9**, 021053 (2019).
- [14] Xiang, J. et al. Giant magnetic quantum oscillations in the thermal conductivity of TaAs: indications of chiral zero sound. *Phys. Rev. X* **9**, 031036 (2019).
- [15] Moll, P. J. W. et al. Magnetic torque anomaly in the quantum limit of Weyl semimetals. *Nat. Commun.* **7**, 12492 (2016).
- [16] Zhang, C.-L. et al. Non-saturating quantum magnetization in Weyl semimetal TaAs. *Nat. Commun.* **10**, 1028 (2019).
- [17] dos Reis, R. D. et al. On the search for the chiral anomaly in Weyl semimetals: the negative longitudinal magnetoresistance. *N. J. Phys.* **18**, 085006 (2016).
- [18] Ramshaw, B. J. et al. Quantum limit transport and destruction of the Weyl nodes in TaAs. *Nat. Commun.* **9**, 2217 (2018).
- [19] Arnold, F. et al. Chiral Weyl pockets and Fermi surface topology of the Weyl semimetal TaAs. *Phys. Rev. Lett.* **117**, 146401 (2016).
- [20] Michenaud, J.-P., Heremans, J., Shayegan, M. & Haumont, C. Magnetostriction of bismuth in quantizing magnetic fields. *Phys. Rev. B* **26**, 2552-2559 (1982).
- [21] KÜchler, R., Bauer, T., Brando, M. & Steglich, F. A compact and miniaturized high resolution capacitance dilatometer for measuring thermal expansion and magnetostriction. *Rev. Sci. Instrum.* **83**, 095102 (2012).
- [22] KÜchler, R. et al. Thermodynamic evidence for valley-dependent density of states in bulk bismuth. *Nat. Mater.* **13**, 461-465 (2014).
- [23] Mikitik, G. P. & Sharlai, Yu. V. Magnetic susceptibility of topological nodal semimetals. *Phys. Rev. B* **94**, 195123 (2016).

- [24] Mikitik, G. P. & Sharlai, Yu. V. Analysis of Dirac and Weyl points in topological semimetals via oscillation effects. *Low Temp. Phys.* **47**, 312-317 (2021).
- [25] Mikitik, G. P. & Sharlai, Yu. V. Manifestation of Berry's phase in metal physics. *Phys. Rev. Lett.* **82**, 2147-2150 (1999).
- [26] Juraszek J. et al. Nonsaturating extreme magnetoresistance and large electronic magnetostriction in LuAs. *Phys. Rev. Research* **1**, 032016(R) (2019).
- [27] Lv, B. Q. et al. Observation of Weyl nodes in TaAs. *Nat. Phys.* **11**, 724-727 (2015).
- [28] Huang, X. et al. Observation of the chiral-anomaly-induced negative magnetoresistance: in 3D Weyl semimetal TaAs. *Phys. Rev. X* **5**, 031023 (2015).
- [29] Li, Z. et al. Weyl semimetal TaAs: crystal growth, morphology, and thermodynamics. *Cryst. Growth Des.* **16**, 1172-1175 (2016).
- [30] Harris, C. R. et al. Array programming with NumPy. *Nature* **585**, 357-362 (2020).
- [31] Jones, E., Oliphant, T., Peterson, P. SciPy: Open source scientific tools for Python. <https://www.scipy.org/> (2001).
- [32] Johansson, F. et al. mpmath: a Python library for arbitrary-precision floatingpoint arithmetic (version 1.2.1). <http://mpmath.org/> (2021).